Supporting Information

Polyoxomolybdate-derived carbon-encapsulated multicomponent electrocatalysts for synergistically boosting hydrogen evolution

Xiong Liu,[‡a] Kun Ni,[‡c] Bo Wen,[a] Chaojiang Niu,[*a] Jiashen Meng,[a] Ruiting Guo,[a] Qi Li,[a] Jiantao Li,[a] Yanwu Zhu,[c] Xiaojun Wu,[*b] Dongyuan Zhao[a,d] and Liqiang Mai[*a]

[a]State Key Laboratory of Advanced Technology for Materials Synthesis and Processing, International School of Materials Science and Engineering, Wuhan University of Technology, Luoshi Road 122, Wuhan, 430070, Hubei, China. E-mail: niuchaojiang11@whut.edu.cn; mlq518@whut.edu.cn

[b]CAS Key Laboratory of Materials for Energy Conversion, CAS Center for Excellence in Nanoscience, Hefei National Laboratory of Physical Sciences at the Microscale, and Synergetic Innovation of Quantum Information & Quantum Technology, University of Science and Technology of China, Hefei, Anhui 230026, P. R. China. E-mail: xjwu@ustc.edu.cn

[c]CAS Key Laboratory of Materials for Energy Conversion, Chinese Academy of Sciences, & Department of Materials Science and Engineering, & iChEM (Collaborative Innovation Center of Chemistry for Energy Materials), University of Science and Technology of China, 96 Jin Zhai Rd, Hefei, Anhui 230026, P. R. China

[d]Department of Chemistry, State Key Laboratory of Molecular Engineering of Polymers, Shanghai Key Laboratory of Molecular Catalysis and Innovative Materials, iChEM, Fudan University, Shanghai 200433, P. R. China

Experimental section

Synthesis of organic-inorganic hybrid polyoxomolybdate composites. In a typical synthesis of MoNi-2-mim nanowire arrays, 0.3 g of $(NH_4)_6Mo_7O_{24}\cdot 4H_2O$, 0.2 g of $Ni(NO_3)_2\cdot 6H_2O$ and 0.5 g of 2-Methylimidazole were added into 40 mL of methanol solution. After stirring for 5 min, the mixture was put into a 50 mL Teflon-lined stainless steel autoclave. Pieces of carbon clothes (20 mm × 30 mm) were washed by diluted hydrochloric acid, deionized water, acetone, ethanol, and dried at 70 °C in a vacuum oven. Afterwards, a piece of pre-treated carbon cloth was placed vertically in an autoclave heated at 160 °C for 20 h. After reacting, the precipitates and carbon cloth were washed with ethanol and dried at 70 °C. The areal weight loading of MoNi-2-mim nanowires on the carbon cloth is ~ 1.5 mg cm^{-2}.

Synthesis of MoO_2-Ni@NC nanowire catalyst. The synthesized MoNi-2-mim nanowire arrays and powders were firstly heated at 280 °C in Ar/H_2 (95:5 vol.%) for 2 h, and then at 500 ~ 600 °C in Ar/H_2 for 2 h to obtain MoO_2-Ni@NC nanowire arrays

and MoO_2-Ni@NC powders. The areal weight loading of MoO_2-Ni@NC nanowires on the carbon cloth is ~ 1 mg cm^{-2}.

Synthesis of MoO_2@NC catalyst. The as-synthesized MoNi-2-mim nanowire arrays were firstly heated at 280 °C in Ar/H_2 for 2 h to maintain the nanowire structure, then at 500 °C in Ar/H_2 for 2 h and Ni component was removed via acid treatments to obtain MoO_2@NC catalyst. Noting that after calcinations at 500 °C, the MoO_2 phase was formed. Lower calcination temperature resulted in lower graphitization degree of carbon, thus the unprotected Ni nanoparticles were easily removed.

Synthesis of NC catalyst. The as-synthesized MoNi-2-mim nanowire arrays were firstly heated at 280 °C in Ar/H_2 for 2 h to maintain the nanowire structure, then calcined at 400 °C in Ar/H_2 for 2 h. The Ni and Mo species were removed via acid treatments and then calcined at 500, 550 or 600 °C to obtain N-doped carbon catalyst. Noting that after calcination at 400 °C, the sample is low-crystalline and the Ni and Mo species can be easily removed.

Characterization. TEM, high-resolution TEM (HRTEM), HAADF-STEM and SAED were collected using a JEM-2100F/Titan G260-300 transmission electron microscope. The crystallographic characterizations of the as-synthesized samples were performed using a Bruker D8 Advance X-ray diffractometer with Cu Kα radiation (λ = 1.54060 Å). SEM images were collected with a JEOL-7100F microscope at an acceleration voltage of 20 kV. XPS and UPS measurements were conducted using an ESCALAB 250Xi instrument. Raman and Fourier-transform infrared (FTIR) spectra were obtained using Renishaw INVIA micro-Raman spectroscopy and Nicolet6700 measurements, respectively. CHNS elemental analyzer was applied to determine the contents of carbon and nitrogen. ICP measurements were performed by PerkinElmer Optima 4300DV spectrometer.

Electrochemical measurements. Electrochemical measurements were measured using a three-electrode system on an electrochemical workstation (CHI760E) in 0.5 M H_2SO_4 solution at room temperature (25 ± 2 °C). A saturated calomel electrode (SCE, saturated KCl as the filling solution) was applied as a reference electrode, a graphite rod was used as a counter electrode and the catalysts supported on the carbon cloth were directly used as a working electrode. LSV polarization curves were tested at a slow scan rate of 5 mV s^{-1} to eliminate the capacitive current during the electrocatalytic reaction as much as possible. The data were corrected by iR compensation to remove the influence of ohmic resistance. EIS was carried out in a frequency range from 0.1 Hz to 100,000 Hz. The commercial Pt/C catalyst supported on the carbon cloth was prepared via

dispersing 8 mg Pt/C and 2 mg Vulcan XC-72R in 700 μL isopropyl alcohol, 250 μL H_2O and 50 μL Nafion solution (5 wt.%) to form a homogeneous ink, then a 125 μL ink which contains 1 mg catalyst was coated on the carbon cloth within 1 cm^2. In 0.5 M H_2SO_4, the potential was referenced to a reversible hydrogen electrode (RHE) based on the following equation: $E(RHE) = E(SCE) + 0.2415\,V + 0.0592 \times pH$. In addition, the current density calculation is based on the geometric area of an electrode.

The proton adsorption experiments were measured by a dialysis method according to the previous reports.[1,2] In detail, the solution which contains the catalyst was dialyzed using a semi-permeable membrane (MWCO 1000) in a 600 mL beaker, and the dialysate was 5 mM HCl (500 mL). If the catalyst displays the good H^+ adsorption behavior, the H^+ would gradually cross the semi-permeable membrane dialyze into the solution of catalyst. After stirring on predetermined time intervals, the residual concentration of HCl solution was determined by titrating with 5 mM NaOH solution. The amount of the adsorbed H^+ (based on the quality of HCl) Q (mg/g) is calculated by the following equation:

$$Q = \frac{(C_0 - C_e) \times V}{W}$$

Here, C_0 and C_e are the initial and equilibrium concentration of HCl (mg/L), respectively. V is the volume of HCl solution (L) and W is the weight (mg) of catalyst adsorbent.

Calculation method. The structure optimization and electron structure calculations of all considered catalysts were performed by using Vienna ab initio simulation package (VASP).[3] A generalized gradient approximation (GGA) with the Perdew-Burke-Ernzerhof (PBE) function was used to describe exchange correlation interactions.[4,5] The plane wave basis set cutoff energy was 500 eV. Gaussian smearing with sigma value of 0.05 eV for the geometry optimization and 0.2 eV for the projected density of states (PDOS) calculation was employed. The energy convergence tolerance for self-consistent field (SCF) for the geometry optimization was 0.01 meV. The force convergence tolerance for the geometry optimization was considered as 0.05 eV/angstrom. All calculations were done with spin unrestricted. The crystal orbital Hamilton population (COHP) calculations were carried out by LOBSTER software program.[8] The K points were sampled as $2 \times 1 \times 1$ using Monkhorst-Pack method[7] for the geometry optimization and sampled as $4 \times 2 \times 1$ for the band decomposed charge density calculation and COHP analyses and sampled as $8 \times 4 \times 1$ for the PDOS calculation.

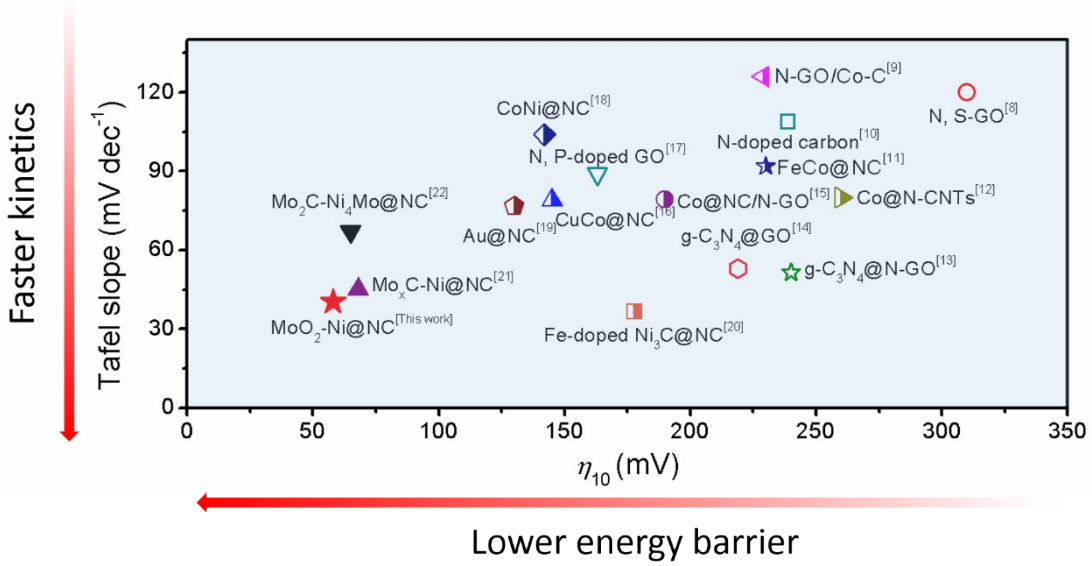

Fig. S1 Comparison of the MoO_2-Ni@NC nanowire catalyst in this work with the carbon-encapsulated catalysts reported previously for the acidic HER. The NC, GO and CNTs represent N-doped carbon, graphene oxide and carbon nanotubes, respectively.

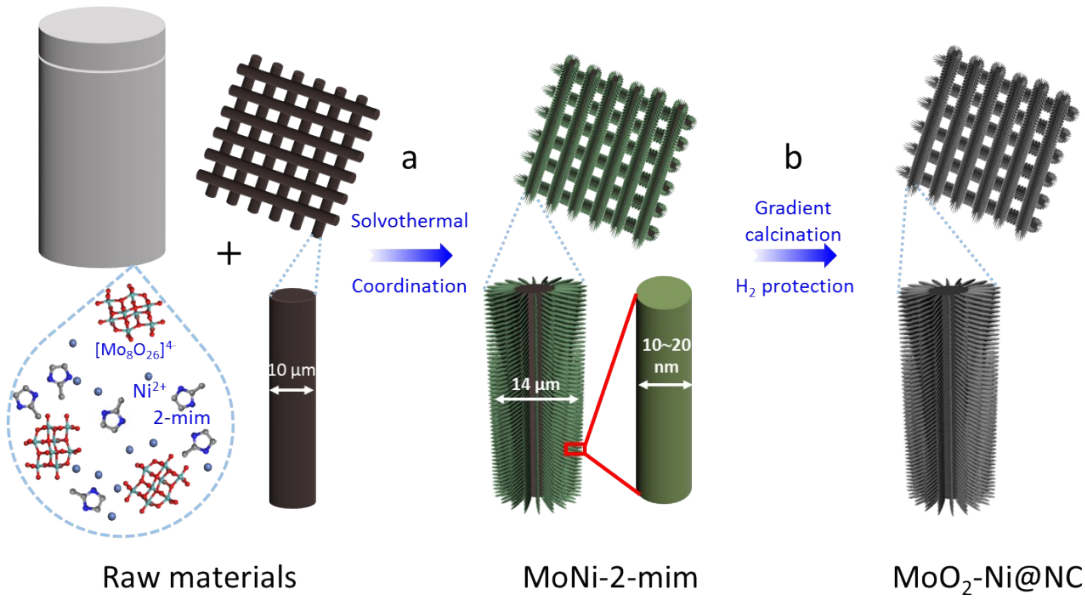

Fig. S2 (a) Synthesis of the novel inorganic-organic hybrid polyoxomolybdate (denoted as MoNi-2-mim) nanowire arrays. (b) Formation of the N-doped carbon-encapsulated MoO_2-Ni (denoted as MoO_2-Ni@NC) nanowire arrays via the calcination under H_2 protection.

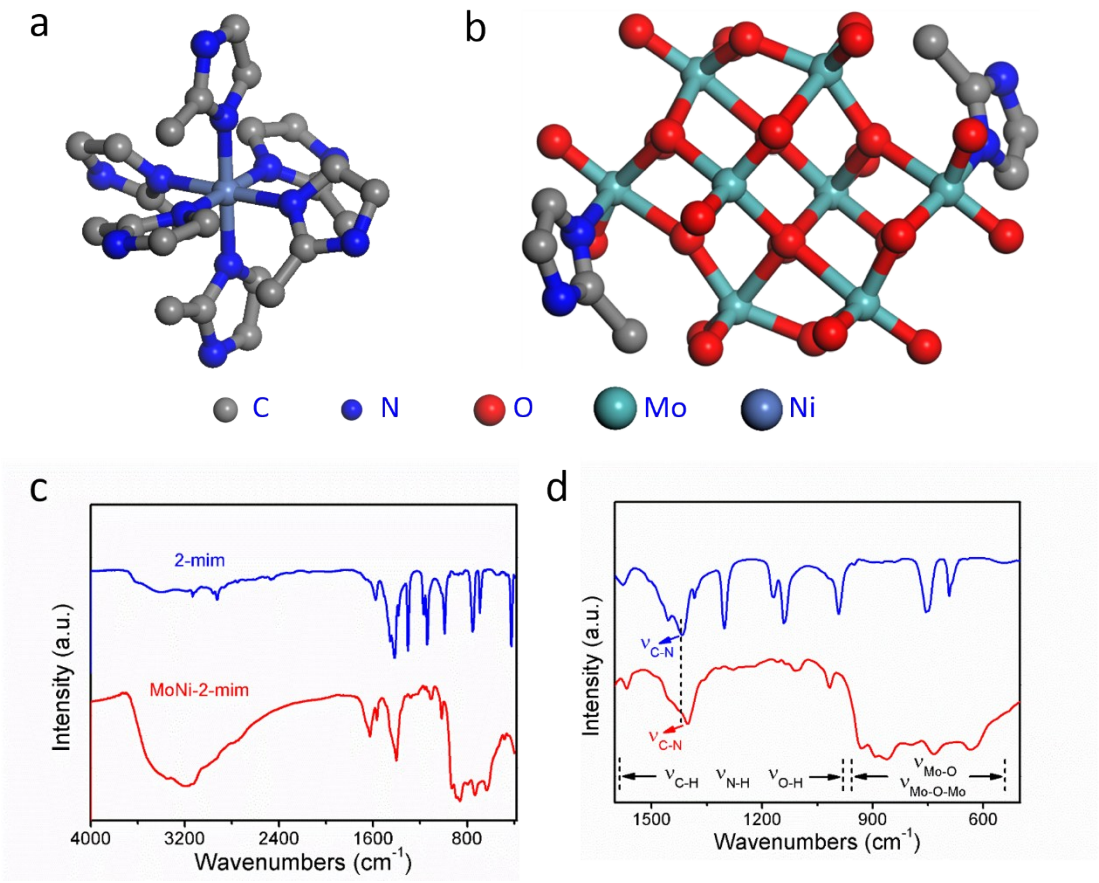

Fig. S3 The structures of (a) $[Ni(2\text{-mim})_6]^{2+}$ cation and (b) $[(2\text{-mim})_2Mo_8O_{26}]^{4-}$ anion. (c,d) FTIR spectra of the 2-mim and MoNi-2-mim powders.

Fig. S3c shows broad peaks at ~ 3200 cm^{-1}, which origins from stretching vibrations OH of the physical absorbed water, C-H and N-H functional groups of the 2-mim ligands. The peaks from 1070 to 1650 cm^{-1} can be assigned to the bending vibrations of the C-H, N-H, O-H and C-N. And the broad and strong peaks at 931 and 892 cm^{-1} can be attributed to the Mo-O stretching, while those peaks from 650 to 850 cm^{-1} are assigned to the Mo-O-Mo bending vibrations. No peak at about 570 cm^{-1} can be found. All above vibrational features can demonstrate the existence of the $[Mo_8O_{26}]^{4-}$ anions. In addition, the red-shift of 18 cm^{-1} for the C-N stretching in MoNi-2-mim nanowires composition indicates that the 2-mim ligands have coordinated to nickel ions by means of nitrogen atoms.

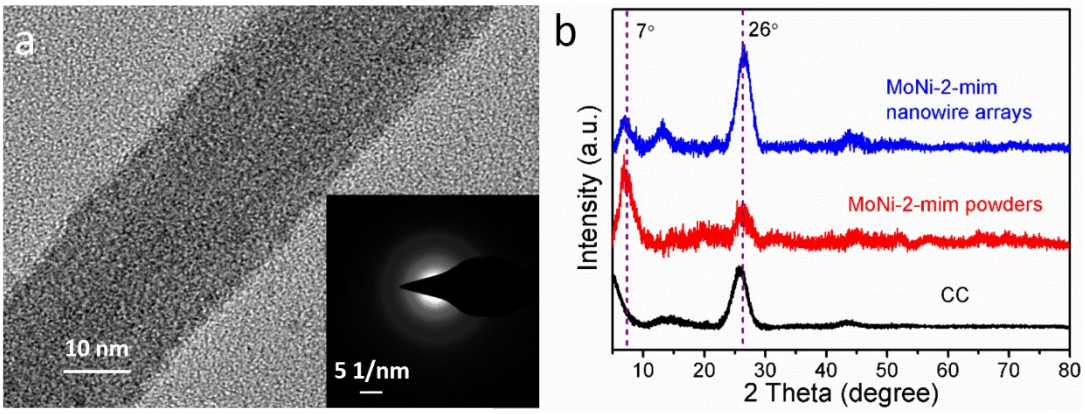

Fig. S4 (a) TEM image of a single MoNi-2-mim nanowire and the inset is the corresponding SAED. (b) XRD patterns of the carbon cloth, MoNi-2-mim powders and MoNi-2-mim nanowire arrays.

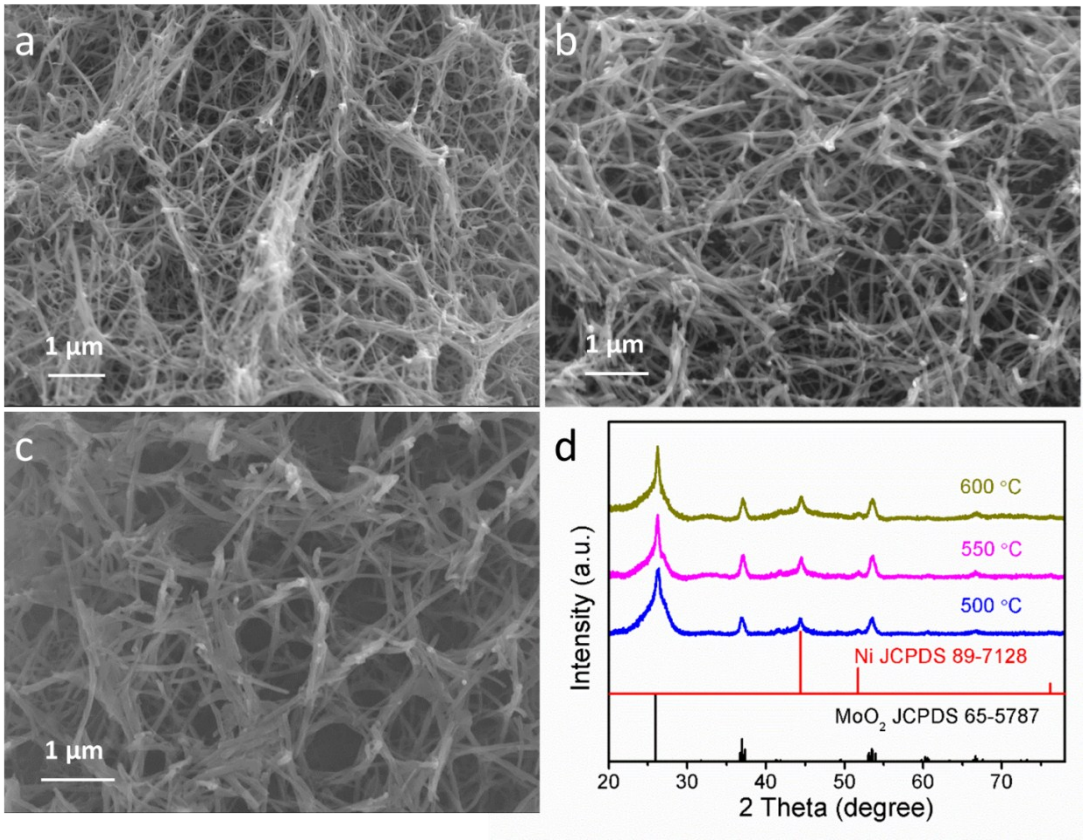

Fig. S5 (a-c) SEM images of the MoO_2-Ni@NC nanowire arrays after calcination at (a) 500, (b) 550 and (c) 600 °C. (d) XRD patterns of the MoO_2-Ni@NC nanowire arrays after calcination. The broad peak at ~ 26° belongs to the diffraction peaks of the carbon cloth.

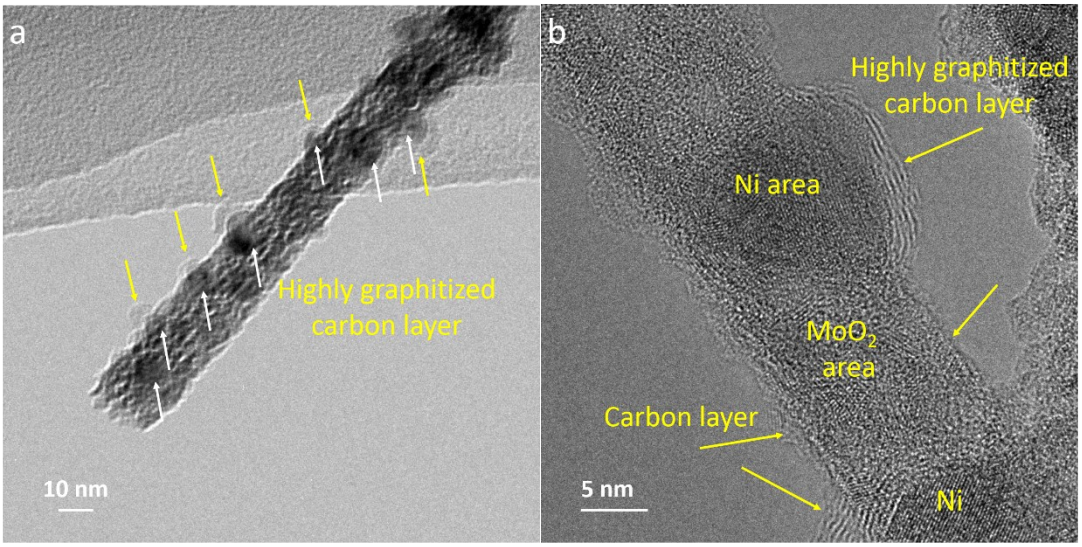

Fig. S6 (a) TEM and (b) HRTEM images of a single MoO_2-Ni@NC nanowire.

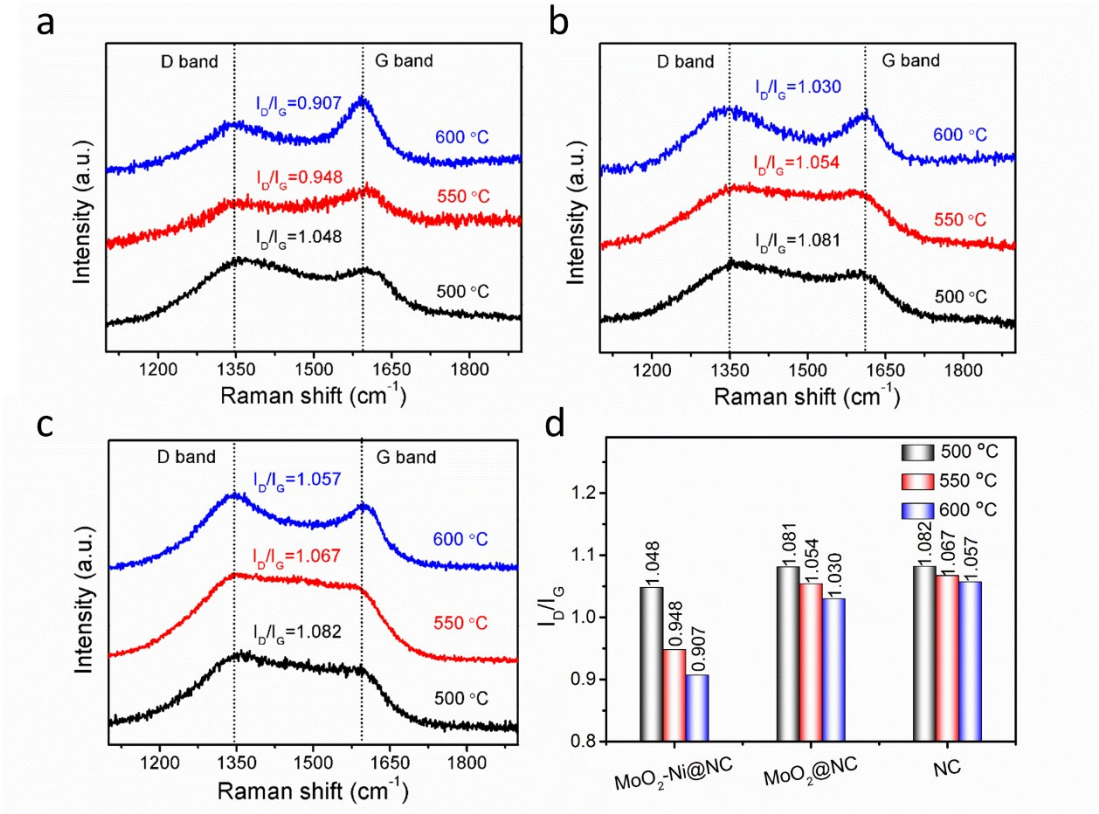

Fig. S7 Raman spectra of (a) MoO_2-Ni@NC, (b) MoO_2@NC and (c) NC samples at various calcination temperatures. (d) The corresponding I_D/I_G values.

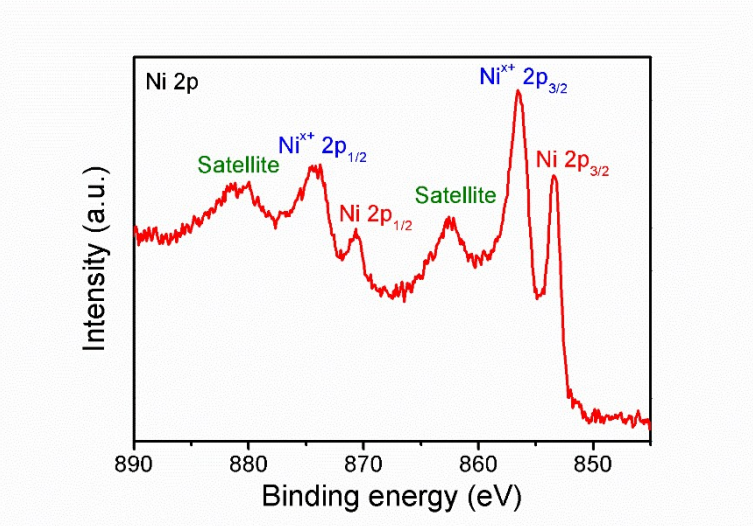

Fig. 8 XPS spectrum of Ni 2p for MoO_2-Ni@NC nanowires.

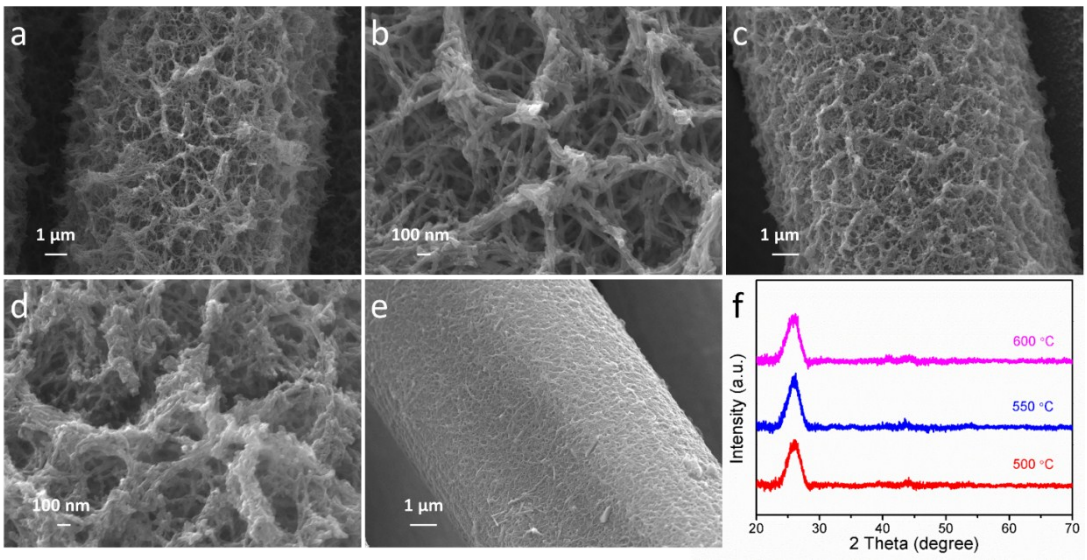

Fig. S9 Morphology and phase characterizations of the N-doped carbon on the carbon cloth. (a-e) SEM images of the N-doped carbon on the carbon cloth after calcination at different temperatures in Ar/H_2, (a, b) 500 °C, (c, d) 550 °C and (e) 600 °C. (f) XRD patterns of the N-doped carbon on the carbon cloth after calcination at 500, 550 and 600 °C. The broad peak at ~ 26° belongs to the diffraction peaks of the carbon cloth.

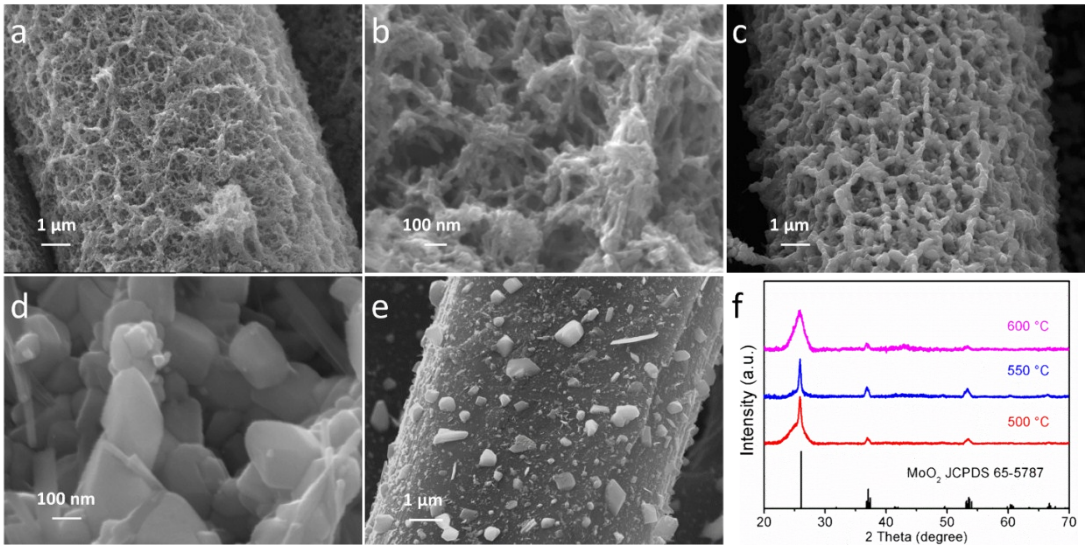

Fig. S10 (a-e) SEM images of the MoO_2@NC on the carbon cloth after calcination at different temperatures in Ar/H_2. (a, b) 500 °C, (c, d) 550 °C and (e) 600 °C. (f) XRD patterns of MoO_2@NC on the carbon cloth after calcination at 500, 550 and 600 °C. The broad peak at ~ 26° belongs to the diffraction peaks of the carbon cloth.

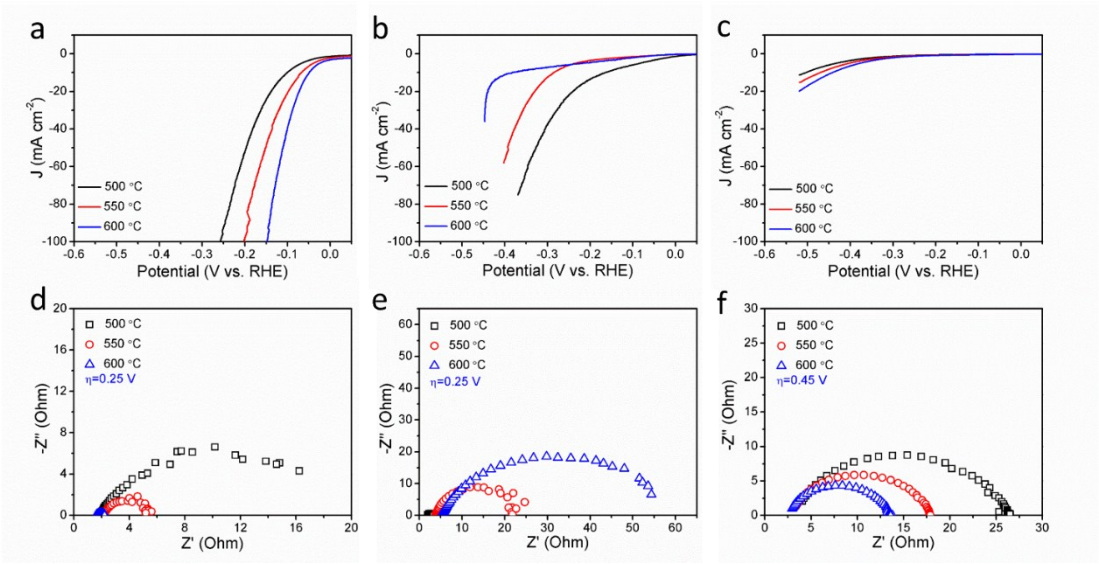

Fig. S11 LSV curves of (a) MoO_2-Ni@NC, (b) MoO_2@NC and (c) NC with various calcination temperatures at 5 mV s^{-1} in 0.5 M H_2SO_4. Nyquist plots obtained by EIS measurements for (d) MoO_2-Ni@NC, (e) MoO_2@NC and (f) NC catalysts with the various calcination temperatures.

We initially investigated the impact of the calcination temperature on the catalytic activity. The morphologies of the MoO_2-Ni@NC nanowire arrays retain well after treated at various calcination temperatures (500, 550 and 600 °C), but not for the MoO_2@NC or NC samples (Fig. S9 and S10). The HER activities of the MoO_2-Ni@NC and NC are improved via an elevated temperature treatment, which may be attributed to the decreased charge transfer resistance. However, the HER activity of the

MoO_2@NC presents dramatic deterioration along with the calcination temperature increasing, which is caused by the severe aggregation and the few active sites.

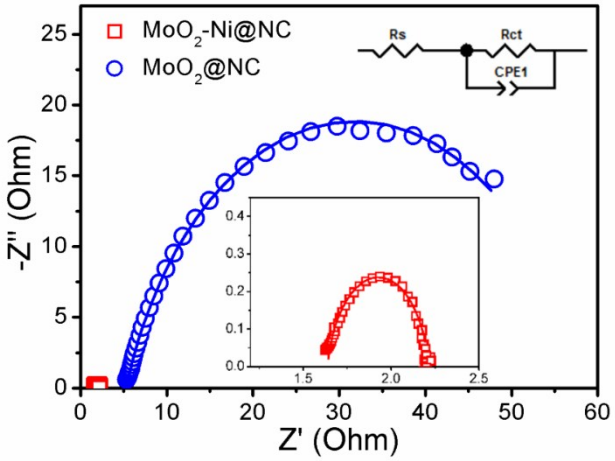

Fig. S12 EIS Nyquist plots of the MoO_2-Ni@NC and MoO_2@NC measured at -0.5 V *vs*. SCE.

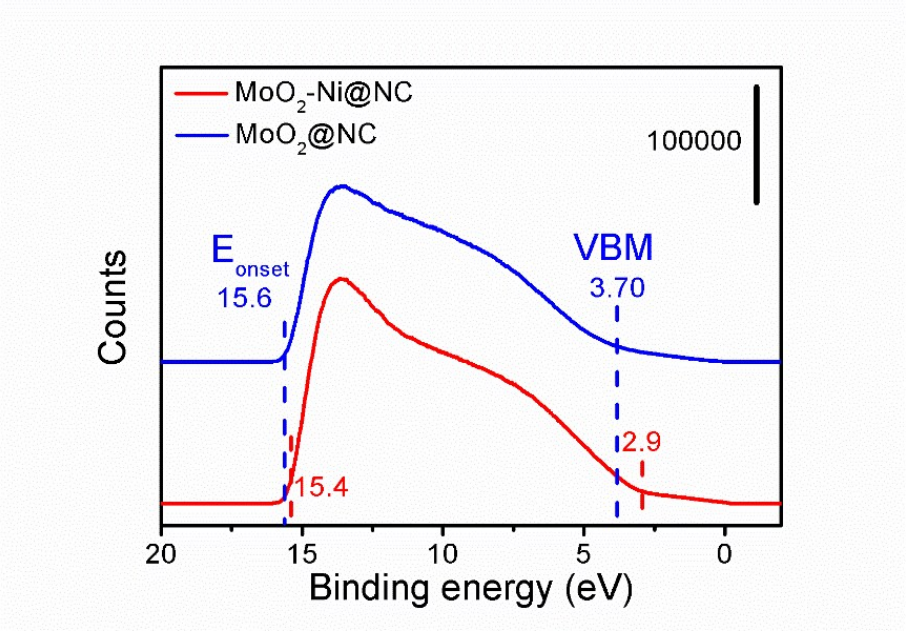

Fig. S13 Valence band spectra of the MoO_2-Ni@NC and MoO_2@NC from UPS measurements.

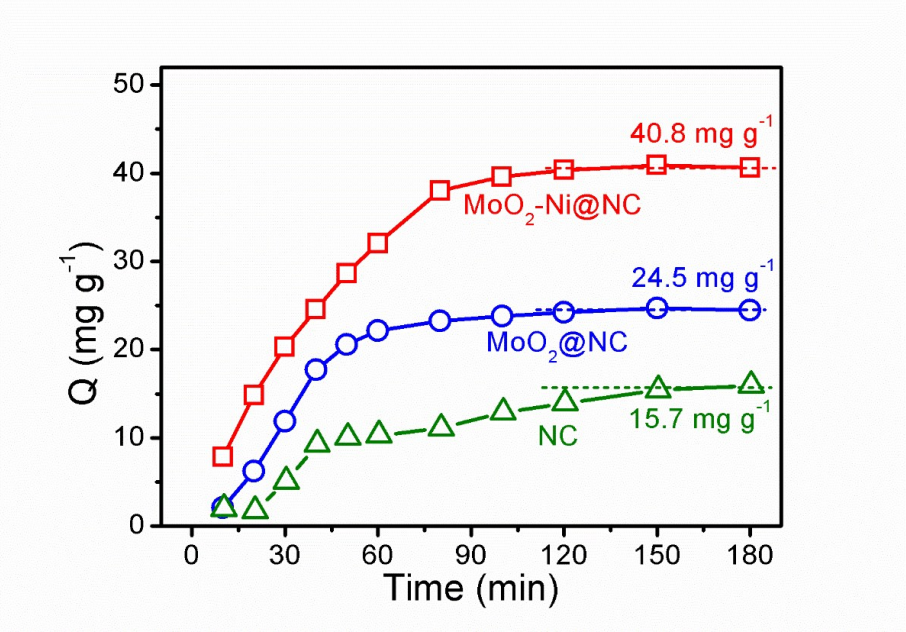

Fig. S14 The dependence of the adsorption time on the amount of adsorbed H^+ (based on the quality of HCl) on the MoO_2-Ni@NC and MoO_2@NC in 5 mM HCl aqueous solution.

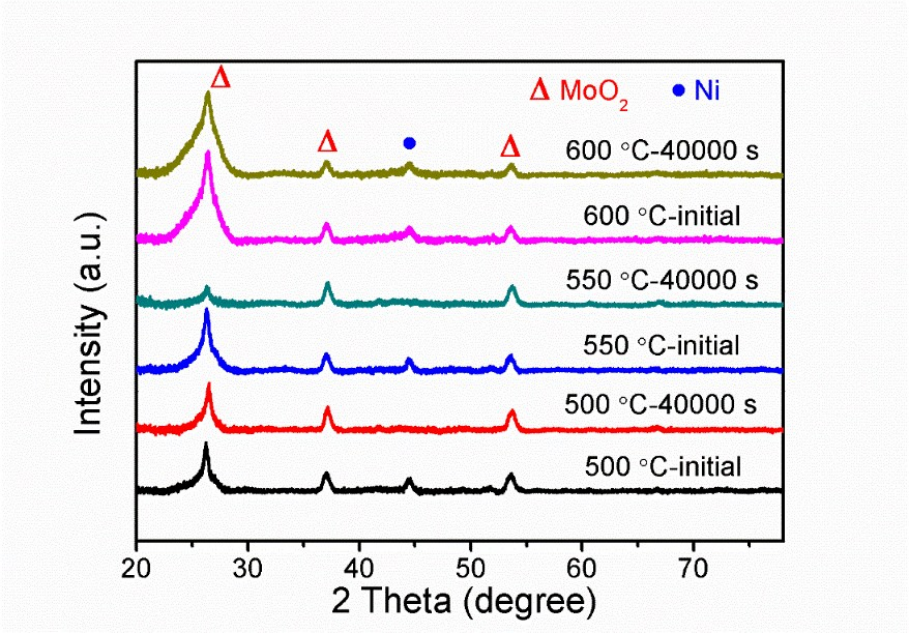

Fig. S15 XRD patterns of the MoO_2-Ni@NC-x (x=500, 550, 600 °C) catalysts tested in 0.5 M H_2SO_4 before and after 40,000 s.

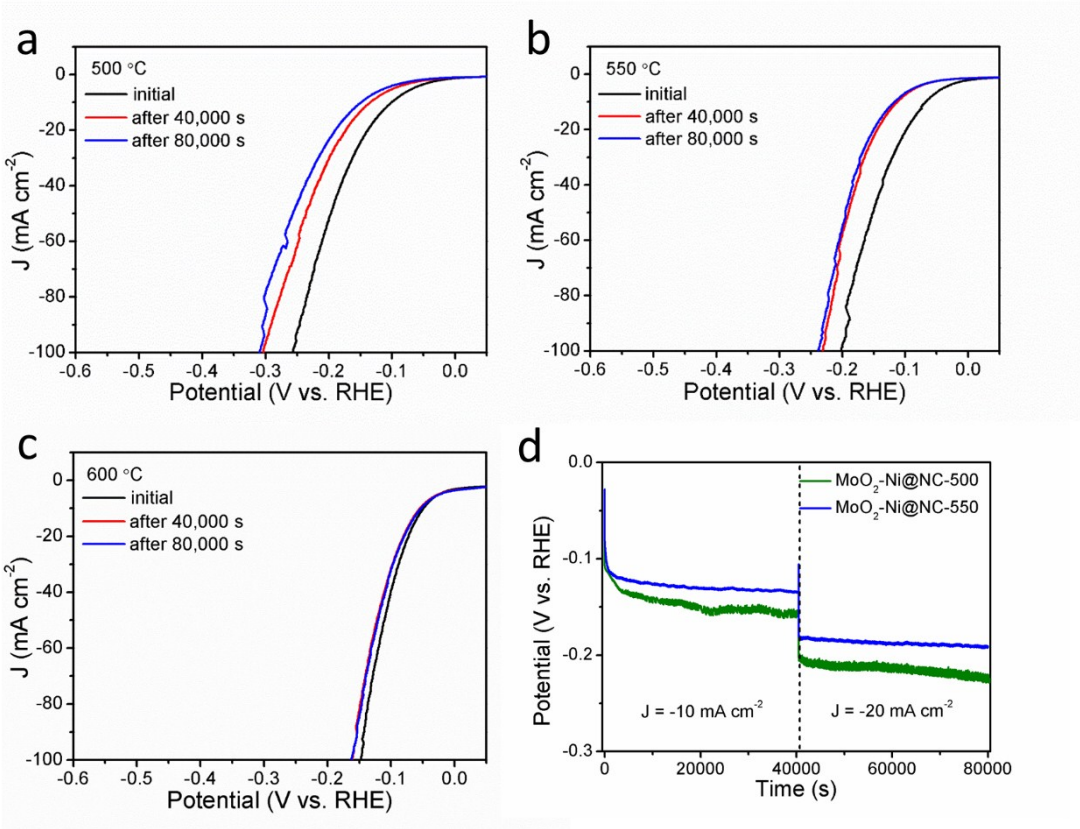

Fig. S16 (a-c) LSV curves of the MoO_2-Ni@NC-x (x = 500, 550 and 600 °C) catalysts tested at a scan rate of 5 mV s^{-1} in 0.5 M H_2SO_4 before, after 40,000 s and 80,000 s, respectively. (d) Galvanostatic measurements of the MoO_2-Ni@NC-500 and MoO_2-Ni@NC-550 catalysts at -10 and -20 mA cm^{-2} in 0.5 M H_2SO_4.

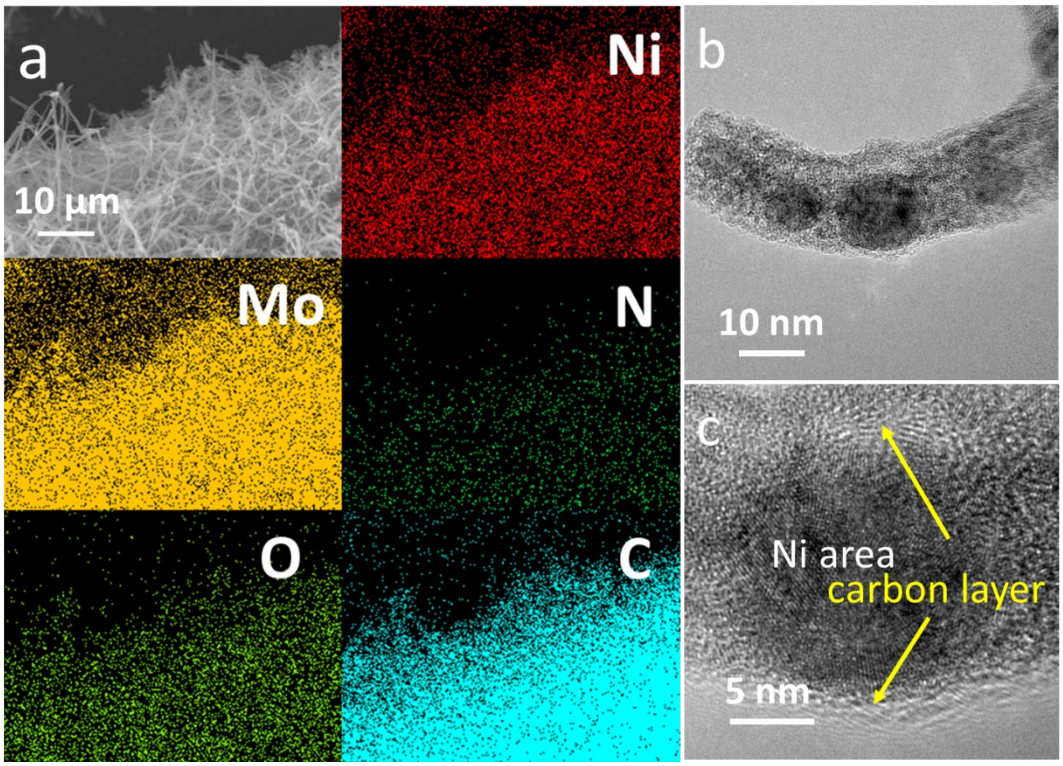

Fig. S17 (a) SEM image and the corresponding elemental mappings of the MoO_2-Ni@NC nanowire arrays after testing in 0.5 M H_2SO_4 for 40,000 s. (b)TEM and (c) HRTEM images of the MoO_2-Ni@NC nanowires, which origin from the MoO_2-Ni@NC nanowire arrays after HER testing in 0.5 M H_2SO_4.

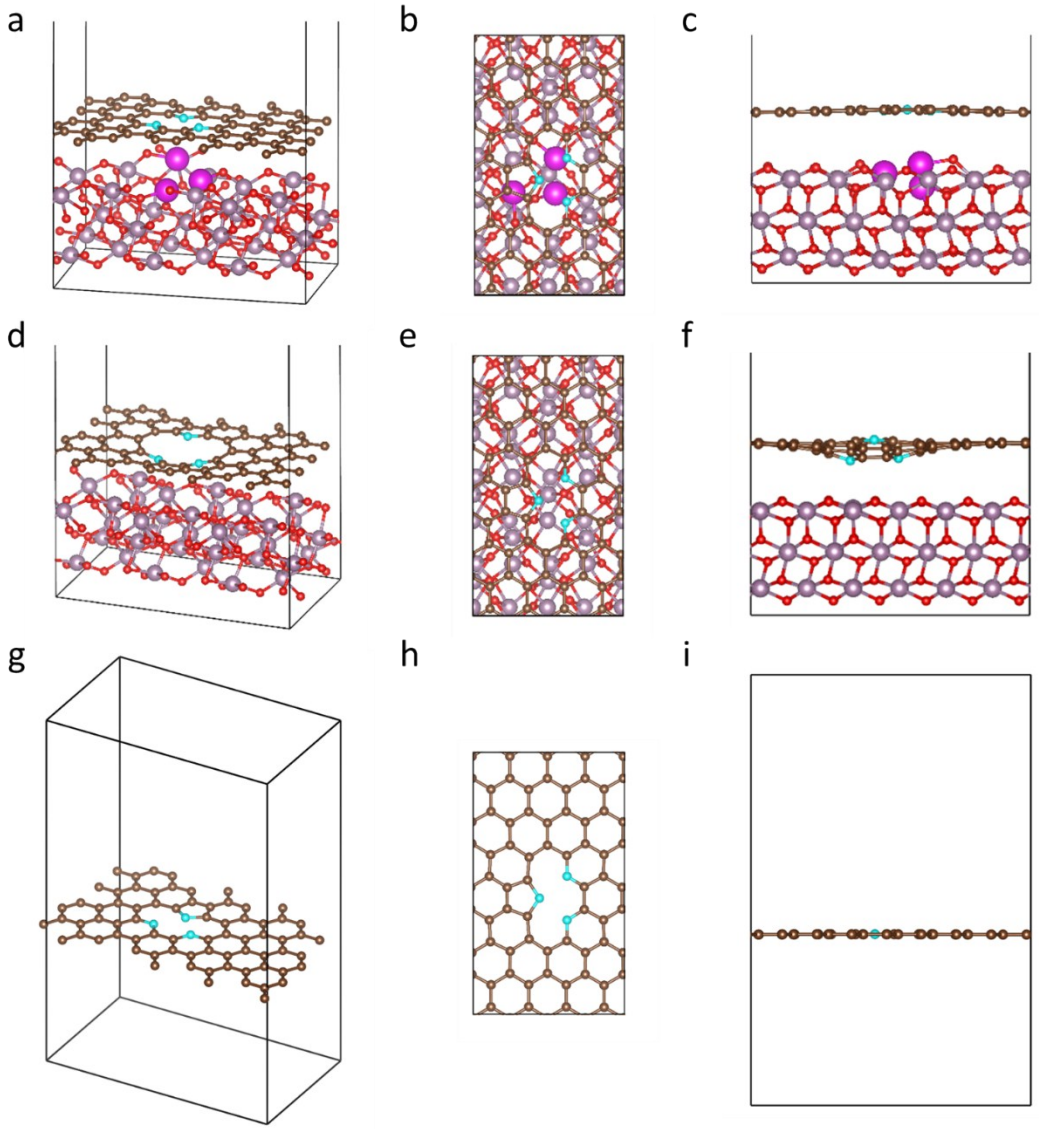

Fig. S18 Structural models of (a-c) MoO_2-Ni@NC, (d-f) MoO_2@NC and (g-i) NC. The blue, brown, red, fuchsia and orchid balls refer to N, C, O, Ni and Mo atoms, respectively.

Based on the approximate plane on our nanowire structure at the atomic level, the planar models are adopted. In addition, due to the single carbon layer is widely used in the models for the carbon-encapsulated electrocatalysts,[15,23,24] thus the planar models with the single N-doped carbon layer on the top and the MoO_2 with Ni cluster substituted partly below the carbon layer were adopted. Though the calculated models are much smaller than the experimental results, it would not undermine the reliability of calculations to reflect the effect of the inner MoO_2-Ni on the outer N-doped carbon.[25,26]

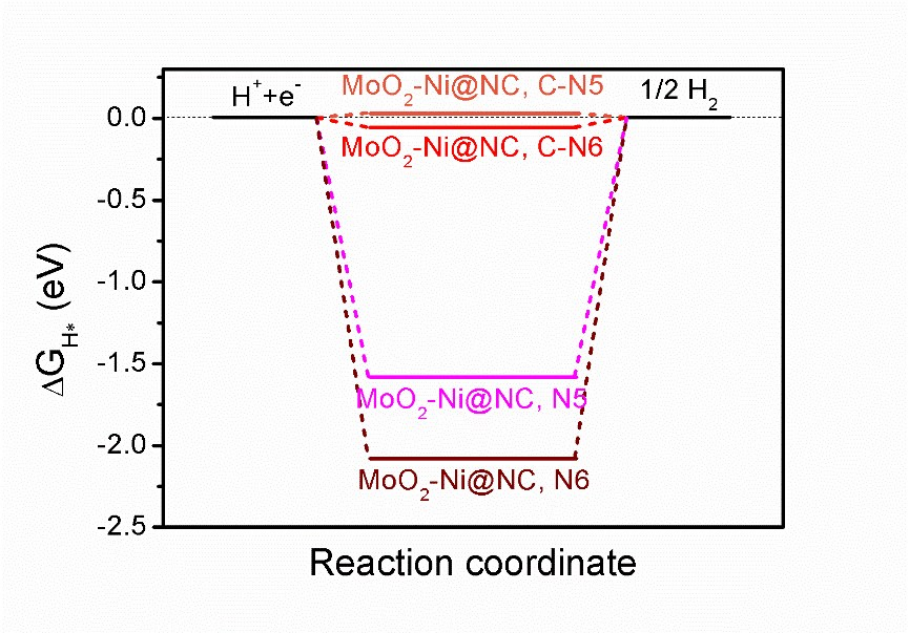

Fig. S19 The ΔG_{H^*} calculated at different sites on the surface of MoO_2-Ni@NC model.

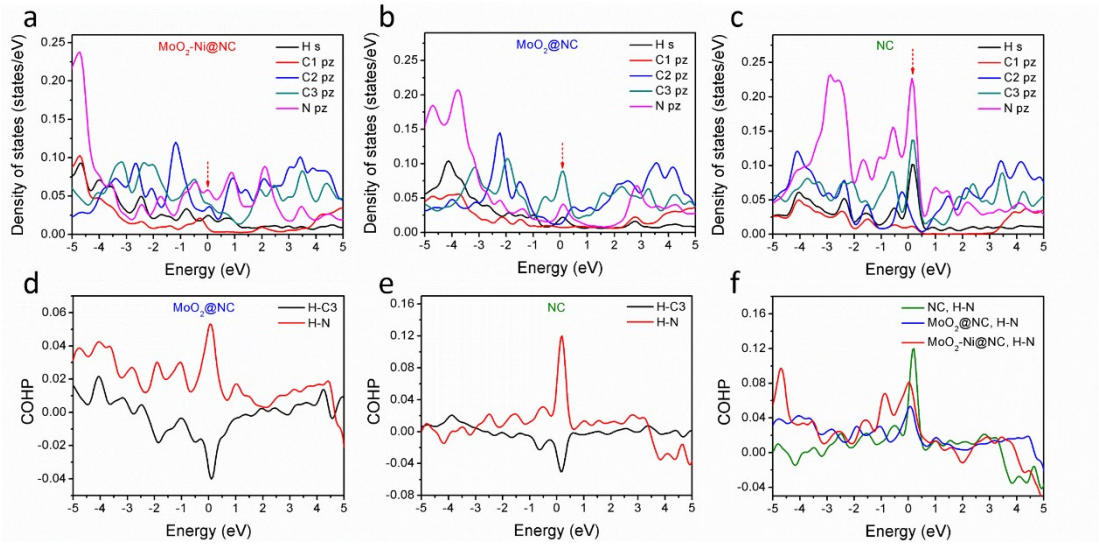

Fig. S20 (a-c) PDOS analysis of MoO_2-Ni@NC, MoO_2@NC and NC models with the H atom adsorbed on the C-N6 site, respectively. (d,e) COHP analysis of MoO_2@NC and NC models, respectively. (f) COHP analysis for the H-N bond of the MoO_2-Ni@NC, MoO_2@NC and NC models, respectively.

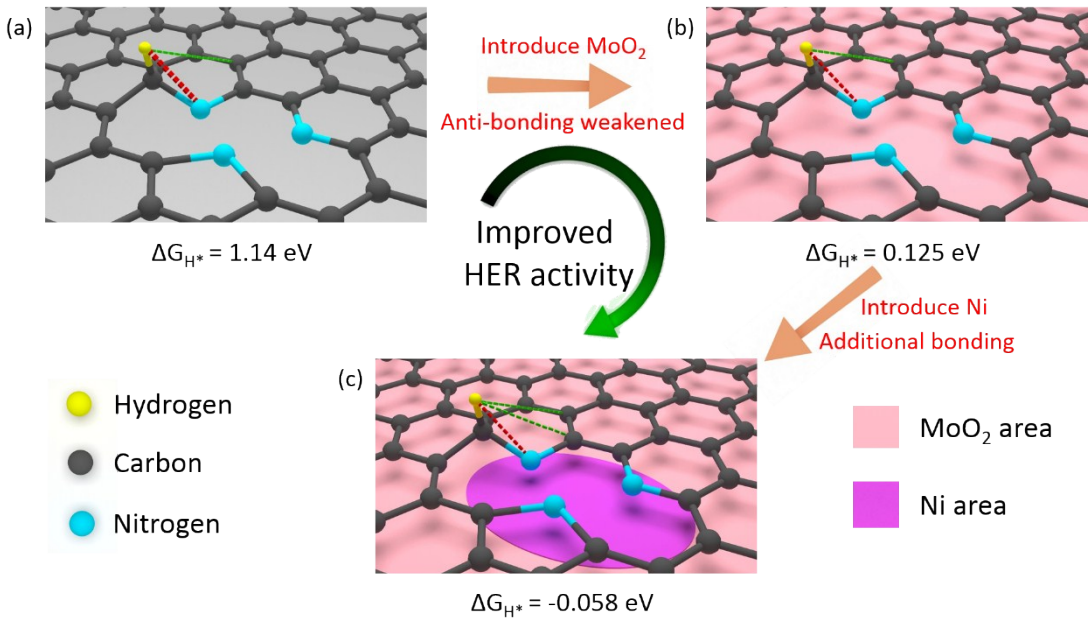

Fig. S21 Schematic diagram of HER-enhanced mechanism. Red dotted line represents anti-bonding and green dotted line represents bonding.

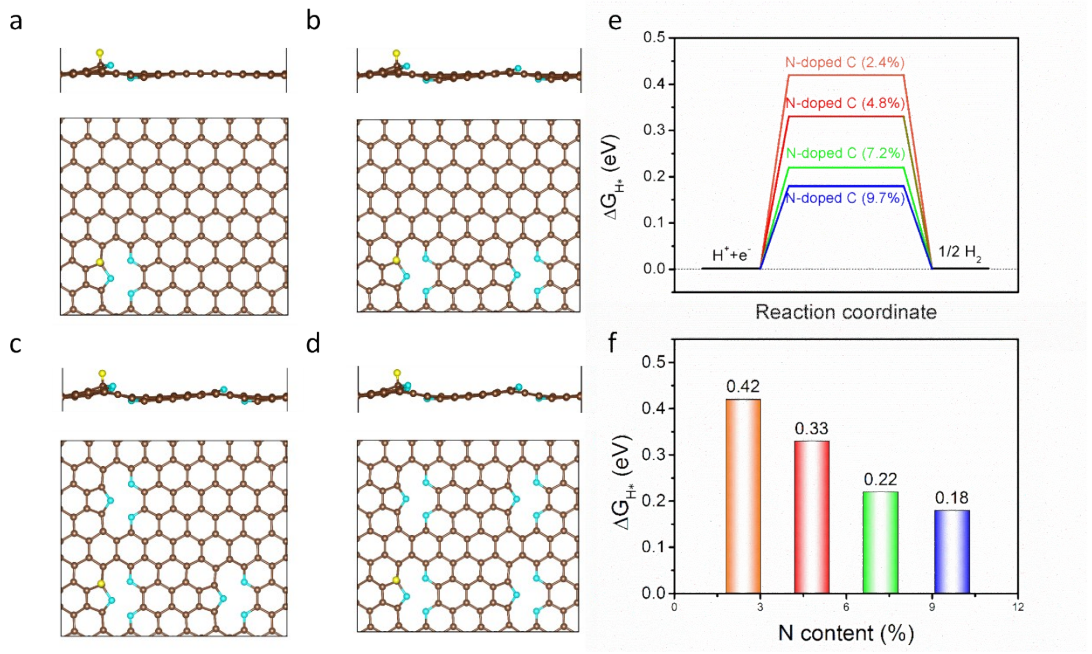

Fig. S22 (a-d) Top views for the different nitrogen content models with H atom adsorbed. The nitrogen content varies from 2.4% atomic percentage to 9.7% atomic percentage in a graphene 8*4 cell. (e,f) The calculated ΔG_{H^*} for the related models in (a) to (d).

It should mentioned that the optimal ΔG_{H^*} value for NC model (0.136 eV) is smaller than the previous reports (~ 0.5 eV),[11,26] and this is attributed to the higher content of doped nitrogen in our model which is agreement with the experimental results.

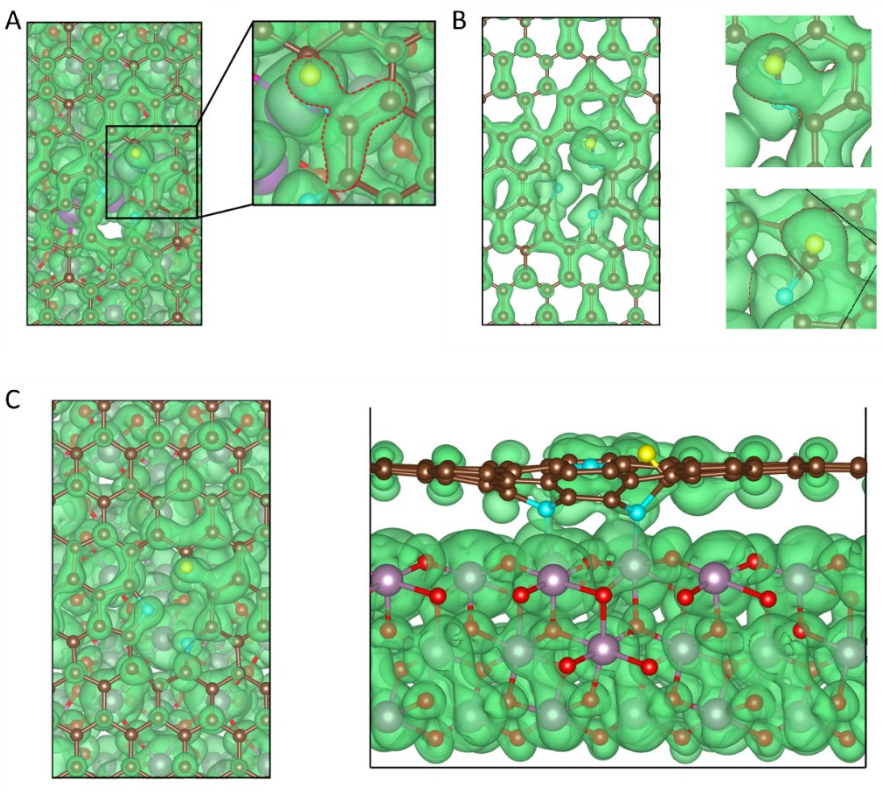

Fig. S23 Band decomposed charge density around Fermi level of MoO_2-Ni@NC (a), NC (b) and MoO_2@NC (c) models with the H atom adsorbed on the C-N6 site, respectively. The yellow, blue, brown, red, fuchsia and orchid balls refer to the H, N, C, O, Ni and Mo atoms, respectively.

Table S1. ICP results of the MoNi-2-mim and MoO_2-Ni@NC powders.

Samples	Mo molar content (%)	Ni molar content (%)
MoNi-2-mim	57.60	42.40
MoO_2-Ni@NC	57.44	42.56

Table S2. CHNS results of the MoNi-2-mim, MoO_2-Ni@NC, MoO_2@NC and NC powders.

Materials	N content (wt.%)	C content (wt.%)	Atom ratios of C and N atoms
MoNi-2-mim	7.75	10.76	1.62
MoO_2-Ni@NC	0.46	4.17	10.57
MoO_2@NC	0.19	8.13	49.92
NC	19.78	74.21	4.38

References

1 H. Li, W. Q. Kong, J. Liu, N. Y. Liu, H. Huang, Y. Liu and Z. H. Kang, *Carbon*, 2015, **91**, 66-75.

2 Y. Y. Ma, C. X. Wu, X. J. Feng, H. Q. Tan, L. K. Yan, Y. Liu, Z. H. Kang, E. B. Wang and Y. G. Li, *Energy Environ. Sci.*, 2017, **10**, 788-798.

3 J. Hafner, *J. Comput. Chem.*, 2008, **29**, 2044-2078.

4 J. P. Perdew, K. Burke and M. Ernzerhof, *Phys. Rev. Lett.*, 1996, *77*, 3865-3868.

5 M. Ernzerhof and G. E. Scuseria, *J. Chem. Phys.*, 1999, **110**, 5029-5036.

6 S. Maintz, V. L. Deringer, A. L. Tchougreeff and R. Dronskowski, *J. Comput. Chem.*, 2016, **37**, 1030-1035.

7 H. J. Monkhorst and J. D. Pack, *Phys. Rev. B*, 1976, **13**, 5188-5192.

8 Y. Jiao, Y. Zheng, K. Davey and S. Z. Qiao, *Nat. Energy*, 2016, **1**, 16130.

9 Y. Hou, Z. H. Wen, S. M. Cui, S. Q. Ci, S. Mao and J. H. Chen, *Adv. Funct. Mater.*, 2015, **25**, 872-882.

10 Y. C. Zhou, Y. H. Leng, W. J. Zhou, J. L. Huang, M. W. Zhao, J. Zhan, C. H. Feng, Z. H. Tang, S. W. Chen and H. Liu, *Nano Energy*, 2015, **16**, 357-366.

11 S. H. Noh, M. H. Seo, J. Kang, T. Okajima, B. Han and T. Ohsaka, *NPG Asia Mater.*, 2016, **8**, e312.

12 X. X. Zou, X. X. Huang, A. Goswami, R. Silva, B. R. Sathe, E. Mikmekova and T. Asefa, *Angew. Chem., Int. Ed.*, 2014, **126**, 4461-4465.

13 Y. Zheng, Y. Jiao, Y. H. Zhu, L. H. Li, Y. Han, Y. Chen, A. J. Du, M. Jaroniec and S. Z. Qiao, *Nat. Commun.*, 2014, **5**, 3783.

14 Q. Han, Z. H. Cheng, J. Gao, Y. Zhao, Z. P. Zhang, L. M. Dai and L. T. Qu, *Adv. Funct. Mater.*, 2017, **27**, 1606352.

15 W. J. Zhou, J. Zhou, Y. C. Zhou, J. Lu, K. Zhou, L. J. Yang, Z. H. Tang, L. G. Li and S. W. Chen, *Chem. Mater.*, 2015, **27**, 2026-2032.

16 M. Kuang, Q. H. Wang, P. Han and G. F. Zheng, *Adv. Energy Mater.*, 2017, **7**, 1700193.

17 J. T. Zhang, L. T. Qu, G. Q. Shi, J. Y. Liu, J. F. Chen and L. M. Dai, *Angew. Chem., Int. Ed.*, 2016, **55**, 2230-2234.

18 J. Deng, P. J. Ren, D. H. Deng and X. H. Bao, *Angew. Chem., Int. Ed.*, 2015, **54**, 2100-2104.

19 W. J. Zhou, T. L. Xiong, C. H. Shi, J. Zhou, K. Zhou, N. W. Zhu, L. G. Li, Z. H. Tang and S. W. Chen, *Angew. Chem., Int. Ed.*, 2016, **128**, 8556-8560.

20 H. S. Fan, H. Yu, Y. F. Zhang, Y. Zheng, Y. B. Luo, Z. F. Dai, B. Li, Y. Zong and Q. Y. Yan, *Angew. Chem., Int. Ed.*, 2017, **56**, 12566-12570.

21 S. P. Wang, J. Wang, M. L. Zhu, X. B. Bao, B. Y. Xiao, D. F. Su, H. R. Li and Y. Wang, *J. Am. Chem. Soc.*, 2015, **137**, 15753-15759.

22 T. Wang, Y. R. Guo, Z. X. Zhou, X. H. Chang, J. Zheng and X. G. Li, *ACS Nan*,

2016, **10**, 10397-10403.

23 J. W. Su, Y. Yang, G. L. Xia, J. T. Chen, P. Jiang and Q. W. Chen, *Nat. Commun.*, 2017, **8**, 14969.

24 P. Jiang, J. T. Chen, C. L. Wang, K. Yang, S. P. Gong, S. Liu, Z. Y. Lin, M. S. Li, G. L. Xia, Y. Yang, J. W. Su and Q. W. Chen, *Adv. Mater.*, 2018, **30**, 1705324.

25 Y. T. Xu, X. F. Xiao, Z. M. Ye, S. L. Zhao, R. A. Shen, C. T. He, J. P. Zhang, Y. D. Li and X. M. Chen, *J. Am. Chem. Soc.*, 2017, **139**, 5285-5288.

26 Y. Yang, Z. Y. Lun, G. L. Xia, F. C. Zheng, M. N. He and Q. W. Chen, *Energy Environ. Sci.*, 2015, **8**, 3563-3571.